



## The Super-Iron Boride Battery

Stuart Licht,<sup>\*,z</sup> Xingwen Yu,<sup>\*</sup> Yufei Wang, and Huiming Wu

Department of Chemistry, University of Massachusetts, Boston, Massachusetts 02125, USA

A high-capacity alkaline redox storage chemistry is explored based on an environmentally benign zirconia-stabilized Fe<sup>6+</sup>/B<sup>2-</sup> chemistry. This super-iron boride battery sustains an electrochemical potential matched to the pervasive, conventional MnO<sub>2</sub>-Zn battery chemistry, but with a much higher electrochemical storage capacity. Whereas a conventional alkaline battery pairs the 2e<sup>-</sup> zinc anode with a 1e<sup>-</sup> MnO<sub>2</sub> cathode, the new alkaline cell couples an 11e<sup>-</sup> boride anode, such as VB<sub>2</sub>, with a 3e<sup>-</sup> storage hexavalent iron cathode. The cell has an open circuit and discharge potential comparable to the conventional, commercial alkaline battery. Based on VB<sub>2</sub> (72.6 g mol<sup>-1</sup>) and the Fe(VI) salt K<sub>2</sub>FeO<sub>4</sub> (198.0 g mol<sup>-1</sup>), the super-iron boride cell has an 11 Faraday theoretical capacity of 369 mAh g<sup>-1</sup>. Added AgO mediates and further facilitates the 3e<sup>-</sup> K<sub>2</sub>FeO<sub>4</sub> reductive charge transfer, and we demonstrate for super-iron boride that over 300 mAh g<sup>-1</sup> is approached experimentally, which is substantially higher than the conventional Zn/MnO<sub>2</sub> alkaline battery with an experimental capacity (to 0.8 V) of 160 mAh g<sup>-1</sup> and a theoretical capacity of 224 mAh g<sup>-1</sup>.

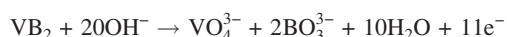
© 2008 The Electrochemical Society. [DOI: 10.1149/1.2839554] All rights reserved.

Manuscript submitted November 9, 2007; revised manuscript received December 26, 2007.  
Available electronically February 20, 2008.

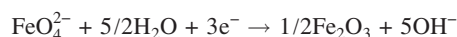
Aqueous Zn-MnO<sub>2</sub> redox charge storage chemistry has been established for over a century and continues as the dominant mechanism of primary electrochemical storage. Capacity, power, cost, and safety factors have led to annual global use on the order of 10<sup>10</sup> primary Zn-MnO<sub>2</sub> batteries.<sup>1</sup> This chemistry is increasingly challenged in meeting the growing energy and power demands of contemporary optical, electromechanical, electronic, and medical consumer devices. Hence, the search for new energy storage chemistry systems, with higher capacity and energy density, has been increasingly emphasized.<sup>1-7</sup>

In 1999, we introduced a cathodic chemistry,<sup>1</sup> which is based on a class of Fe(VI) or "super-iron" oxides with a 3e<sup>-</sup> intrinsic capacity (e.g., K<sub>2</sub>FeO<sub>4</sub>: 406 mAh g<sup>-1</sup>) higher than MnO<sub>2</sub> (308 mAh g<sup>-1</sup>). In 2004 it was reported that metal borides could be used as anodic alkaline charge storage materials.<sup>8,9</sup> However, two obstacles to implementation of this alkaline boride anodic chemistry were evident, in which boride undergoes a 5e<sup>-</sup> oxidation from the -2 to +3 valence state. There is a significant domain in which the boride anode materials corroded spontaneously, generating hydrogen gas, and the electrochemical potential of the boride anodes was less negative than that of zinc. Therefore, a boride MnO<sub>2</sub> cell was subject to decomposition, and the voltage of this cell was low compared to the electrochemical potential of the pervasive Zn-MnO<sub>2</sub> redox chemistry. In a recent communication, we introduced a battery chemistry based on Fe(VI)-boride redox charge transfer, overcoming both obstacles to utilization of the boride alkaline anode.<sup>7</sup> The super-iron cathode provides the requisite additional electrochemical potential, and our recently demonstrated zirconia hydroxide-shuttle overlayer, which stabilizes alkaline charge-transfer chemistry,<sup>6</sup> is also shown to prevent corrosion of the boride anode. Sustaining much higher electrochemical capacity than a conventional MnO<sub>2</sub>-Zn battery, this Fe(VI)-boride alkaline battery chemistry has individual electrode and overall discharge reactions, such as

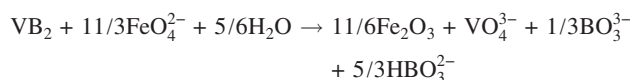
anode:



cathode:



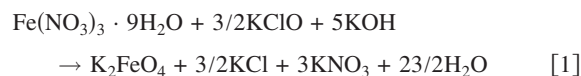
cell:



Here we provide an expanded study of these energetic, super-iron cathode/boride anode alkaline redox couples.

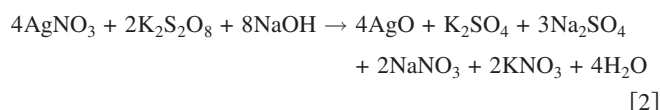
### Experimental

K<sub>2</sub>FeO<sub>4</sub> of 97–98.5% was prepared according to



Preparation and analysis of K<sub>2</sub>FeO<sub>4</sub> has been detailed elsewhere.<sup>10,11</sup> The dried K<sub>2</sub>FeO<sub>4</sub> product is highly stable over a period of years.<sup>10,11</sup> In this study, the K<sub>2</sub>FeO<sub>4</sub> was used as synthesized or, when indicated, after size separation using polypropylene grids (MacMaster-Carr) of various mesh sizes, as salts with various constrained particle sizes, in the size range <28, <35, 35–73, or 73–149 μm.

AgO was prepared by the reaction of an alkaline AgNO<sub>3</sub> solution with K<sub>2</sub>S<sub>2</sub>O<sub>8</sub> at 85 °C, in accordance with standard methods<sup>12</sup>



The boride anode was generally either TiB<sub>2</sub> (Aldrich 10 μm powder) or VB<sub>2</sub> (Aldrich 10 μm/325 mesh powder) (coated or uncoated) as indicated and mixed with the graphite. In addition, TaB (Aldrich), TaB<sub>2</sub> (Aldrich), MgB<sub>2</sub> (Aldrich), CrB<sub>2</sub> (Aldrich), CoB<sub>2</sub> (Aldrich), Ni<sub>2</sub>B (Acros), and LaB<sub>6</sub> (Acros) were also considered.

We have established that a zirconia overlayer stabilizes the alkaline anode and cathode materials.<sup>6,7</sup> A 1% ZrO<sub>2</sub> coating on a powder of either K<sub>2</sub>FeO<sub>4</sub>, TiB<sub>2</sub>, or VB<sub>2</sub> was prepared as follows: 8 mg ZrCl<sub>4</sub> [analytical reagent grade, ACROS] dissolved in 8 mL ether (Fisher) and stirred with 0.8 g of the solid powder in air for 30 min, followed by vertex suction, then vacuum removal of the remaining organic solvent and drying overnight. Analysis of the coating was performed with attenuated total reflectance Fourier transform infrared (ATR/FTIR) spectroscopy using a Nicolet 4700 FTIR with the accessory Smart Orbit diamond crystal and using the Smart Orbit tip. The powder samples (coated material) were compressed into thin pellets, and these pellets were cycled in contact with the diamond crystal by the tip and removed three times to ensure the sample pellet was firmly contacted with the diamond crystal.

Performance, and electrochemical enhancement, of the super-iron boride battery was studied through preparation of button cells containing electrodes with various cathode and anode compositions.

\* Electrochemical Society Active Member.

<sup>z</sup> E-mail: stuart.licht@umb.edu

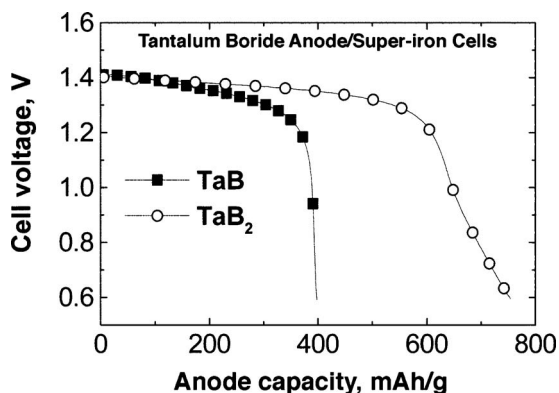


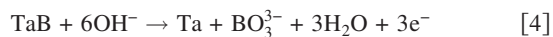
**Figure 1.** Tantalum boride anodes. Super-iron/boride cells which contain either a TaB or a TaB<sub>2</sub> anode are discharged. Anode: 75 wt % TaB<sub>2</sub> (or TaB), 20% graphite, 4.5% KOH, and 0.5% binder (T-30, 30% teflon), combined anode mass: 90 mg. Anode limited conditions are studied by packing each cell, respectively, with excess intrinsic cathode capacity. Cathode: 75% K<sub>2</sub>FeO<sub>4</sub> and 25% graphite. Electrolyte: saturated KOH. The 1 cm button cells are anode capacity limited (cells are configured with a cathode capacity to probe the anode's charge storage limit). The cells are discharged at a constant load of 3 kΩ at 22°C.

Cathodes were composed of K<sub>2</sub>FeO<sub>4</sub> (uncoated or zirconia coated), either with or without indicated additives, and mixed with graphite as a conductor (1 μm graphite, Leico Industries Inc.). For comparison, cells were also alternatively prepared with cathodes containing MnO<sub>2</sub> (electrolytic manganese dioxide, EraChem K60), NiOOH [from a commercial Powerstream Ni-metal hydride (MH) button cell], or KIO<sub>4</sub> (ACROS). Anodes were composed of the indicated borides (uncoated or zirconia coated), either with or without indicated additives, and mixed with the graphite as a conductor (1 μm graphite, Leico Industries Inc.). For comparison, cells were also alternatively prepared with anodes containing metal hydride (from a commercial Powerstream Ni-MH button cell) or Zn gel (from a commercial alkaline Energizer cell). Saturated KOH was used as the electrolyte. Cells were discharged over constant, described load resistances. The potential variation over time was recorded via Lab View Acquisition on a PC. The cumulative discharge was determined by subsequent integration.

## Results and Discussion

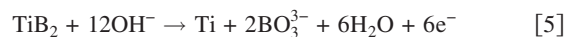
FeB and CoB were previously considered as alkaline boride anodes; however, each was observed to exhibit an anodic capacity less than that of TiB<sub>2</sub> and VB<sub>2</sub>.<sup>9</sup> In this study, we have also considered the borides TaB, TaB<sub>2</sub>, MgB<sub>2</sub>, CrB<sub>2</sub>, CoB<sub>2</sub>, Ni<sub>2</sub>B, and LaB<sub>6</sub> as alternative active anode materials for alkaline electrochemical storage cells. While the two tantalum boride salts exhibit a degree of accessible anodic charge storage capacity, each of the other borides did not exhibit significant primary discharge behavior due to their high solubilities in alkaline solution or their reactivity with alkaline electrolyte.

The electrochemical discharge characteristics of TaB and TaB<sub>2</sub>, as candidate alkaline boride anodes, are summarized in Fig. 1. The alkaline reduction of the TiB<sub>2</sub> anode had been previously shown to be consistent with formation of zero valent titanium,<sup>8,12</sup> and similarly, we expect the reduction of TaB<sub>2</sub> can yield tantalum. According to the half-cell oxidation reaction of TaB<sub>2</sub> (formula weight  $W = 202.57 \text{ g mol}^{-1}$ ) or TaB ( $W = 191.76 \text{ g mol}^{-1}$ ) to a Ta product, the theoretical (intrinsic) anodic reactions of the salts in an alkaline medium are

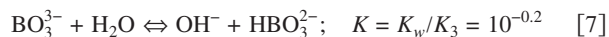
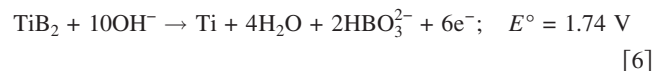


In accordance with Eq. 3 and 4, the intrinsic  $n = 6\text{e}^-$  capacity of TaB<sub>2</sub> and the  $n = 3\text{e}^-$  capacity of TaB anodes are, respectively, 793.8 and 419.3 mAh g<sup>-1</sup>, as determined from a net intrinsic capacity of  $nF/W$  ( $F =$  the Faraday constant). The experimental anodic charge storage constraints of the TaB and TaB<sub>2</sub> anodes are shown in Fig. 1. The anodic capacity is measured by discharge in electrochemical coin cells configured to contain excess (K<sub>2</sub>FeO<sub>4</sub>) cathode capacity. In a balanced manner, later cases in this study probing cathode constraints are measured in cells instead containing excess anode capacity. Unless stated otherwise, the coin cells are generally discharged at low current (constant, high load resistance) to maximize coulombic efficiency and to probe the discharge potential at low overpotential, although significant higher rate discharges are also included later in this study. As seen in Fig. 1, the TaB<sub>2</sub> exhibits an anodic storage capacity comparable to the widely used conventional alkaline zinc anode (820 mAh g<sup>-1</sup>). Compared to the theoretical anodic capacity determined in accordance with Eq. 3, approximately 85% coulombic efficiency was obtained for this TaB<sub>2</sub> anode, reflecting experimental access to a high degree of the 6e<sup>-</sup> intrinsic capacities. Compared to the theoretical capacity determined from Eq. 4, 93% coulombic efficiency was obtained for the TaB anode.

Although the 6e<sup>-</sup> TaB<sub>2</sub> provides higher anodic capacity than the 3e<sup>-</sup> TaB, the 6e<sup>-</sup> titanium boride anode provides even higher accessible capacity.<sup>7</sup> The analogous anodic discharge of the boride TiB<sub>2</sub>, rather than the tantalum diboride-containing alkaline cell, provides a significantly higher gravimetric charge storage capacity to the metal product due to the lighter weight of this metal (47.87 g mol<sup>-1</sup> titanium compared to 180.95 g mol<sup>-1</sup> tantalum), and cell products are generalized as Ti and BO<sub>3</sub><sup>3-</sup>



The small third acid dissociation constant of boric acid (H<sub>3</sub>BO<sub>3</sub> with pK<sub>1,2,3</sub> = 9.1, 12.7, and 13.8) drives spontaneous free hydroxide formation from borate and water in the pH 14 domain. Hence, Eq. 5 is in simultaneous equilibrium with cell products which also include HBO<sub>3</sub><sup>2-</sup>. In this case, the equilibrium between BO<sub>3</sub><sup>3-</sup> and HBO<sub>3</sub><sup>2-</sup> acts as a buffer against hydroxide depletion during anodic discharge



The products vary with hydroxide concentration, degree of hydration, and depth of discharge, including the anhydride product B<sub>2</sub>O<sub>3</sub> and cation containing species, such as in aqueous KOH: K<sub>x</sub>H<sub>z</sub>BO<sub>3</sub><sup>3-x-z</sup> (where  $x$  ranges from 0 to 3 and  $z$  from 0 to 3 -  $x$ ), as well as polymeric species, such as those related to the boric condensation reaction forming borax species K<sub>y</sub>B<sub>4</sub>O<sub>7</sub><sup>2-y</sup>.

In accordance with Eq. 5 or 6 and a formula weight,  $W = 69.5 \text{ g mol}^{-1}$ , TiB<sub>2</sub> has a net intrinsic 6e<sup>-</sup> anodic capacity of 2314 mAh g<sup>-1</sup>. A significant advantage of the titanium boride anode is that it contains higher capacity compared with the conventional alkaline zinc anode (820 mAh g<sup>-1</sup>). As seen in the top of Fig. 2, the observed TiB<sub>2</sub> anode capacity is in excess of 2000 mAh g<sup>-1</sup> at low discharge rates (over a 100 kΩ load discharge in the 1 cm diameter cell) and still in excess of 1300 mAh/g at moderate discharge rates (over a 3 kΩ load).

VB<sub>2</sub> has the highest anode capacity studied. Unlike TiB<sub>2</sub>, the alkaline VB<sub>2</sub> undergoes oxidation of the tetravalent transition metal ion with V<sup>4+</sup> ⇒ V<sup>5+</sup>, as well as oxidation of each of the two borides with B<sup>2-</sup> ⇒ B<sup>3+</sup>, for a net 11e<sup>-</sup> anodic process

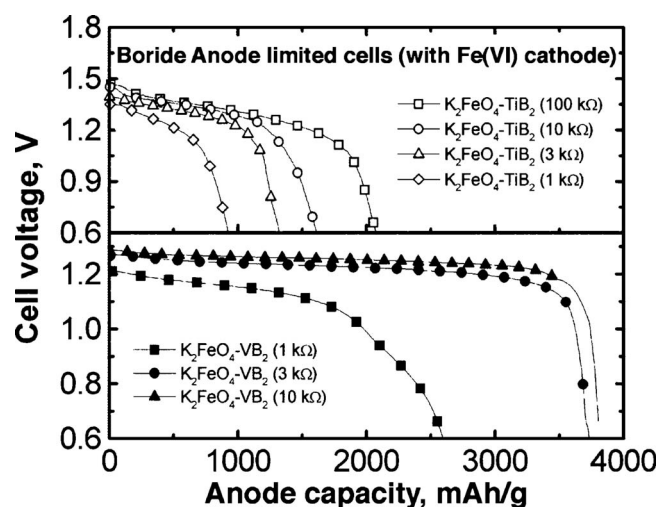
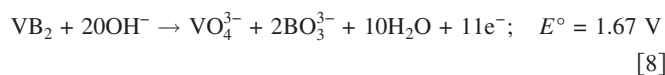


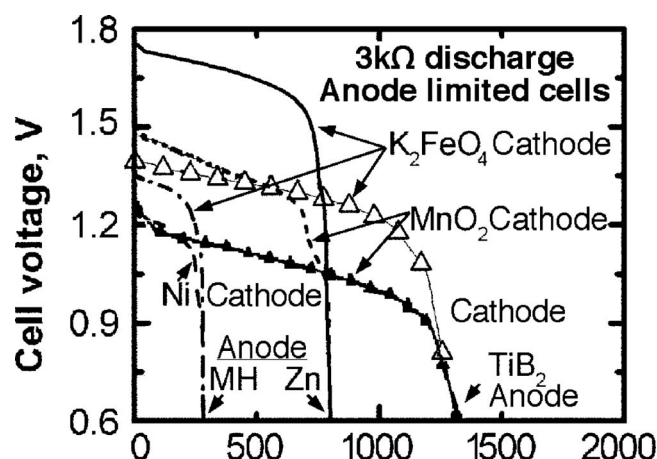
**Figure 2.** Discharge of high-capacity  $\text{TiB}_2$  and  $\text{VB}_2$  boride alkaline anode cells with  $\text{K}_2\text{FeO}_4$  cathodes. Electrolyte and cell conditions are as described in Fig. 1, discharged under the indicated constant ohmic load conditions. Cells contain excess cathode capacity and are limited to either 5 mAh (100 k $\Omega$  load) or 10 mAh (<100 k $\Omega$ ) intrinsic anode capacity to insure discharge in a short time frame (3 weeks or less). (Top)  $\text{TiB}_2$  anode: 75%  $\text{TiB}_2$ , 20% graphite, 4.5% KOH, and 0.5% binder (T-30, 30% Teflon). Cathode: 75%  $\text{K}_2\text{FeO}_4$ , 20% graphite, and 5% KOH. (Bottom) Same cathode; anode: 75 wt %  $\text{VB}_2$ , 20% graphite, 4.5% KOH, and 0.5% binder (T-30, 30% Teflon).



Therefore, in accordance with Eq. 8,  $\text{VB}_2$  has an unusually high, intrinsic  $11\text{e}^-$  anodic capacity of  $11 \text{ F}/(W = 72.6 \text{ g mol}^{-1}) = 4060 \text{ mAh/g}$ , rivaling the high anodic capacity of lithium (3860 mAh/g). The vanadium boride anode  $\text{VB}_2$  has five times the alkaline capacity of zinc. The cell products are generalized in Eq. 8 as  $\text{VO}_4^{3-}$  and  $\text{BO}_3^{3-}$  but, as with the titanium boride discharge, vary with the hydroxide concentration, hydration, and depth of discharge. The speciation of borate and the anhydride salt of boric acid has been previously described ( $\text{H}_3\text{BO}_3$ ,  $\text{H}_2\text{BO}_3^-$ ,  $\text{HBO}_3^{2-}$ ,  $\text{BO}_3^{3-}$ ,  $\text{B}_2\text{O}_3^-$ ,  $\text{K}_x\text{H}_z\text{B}_3\text{O}_3^{3-x-z}$ ,  $\text{K}_y\text{B}_4\text{O}_7^{2-y}$ , and  $\text{B}_2\text{O}_3$ ). In addition, a distribution of vanadate species arises. Vanadate is the deprotonated form of a triprotic acid, vanadic acid ( $\text{H}_3\text{VO}_4$  with  $\text{p}K_{1,2,3} = 3.8, 7.8, \text{ and } 13.0$ ). Equilibrium-driven speciation of  $\text{VO}_4^{3-}$ ,  $\text{HVO}_4^{2-}$ , and  $\text{H}_2\text{VO}_4^-$ , as well as the anhydride product,  $\text{V}_2\text{O}_5$ , and potassium cation species occur.

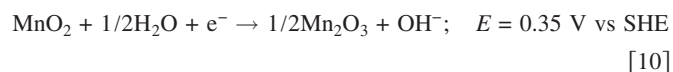
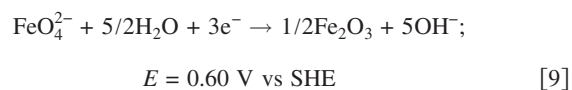
A vanadium, compared with a titanium, diboride salt yields the highest alkaline anodic capacity. As seen in the lower portion of Fig. 2, the  $\text{VB}_2$  anode approaches this high capacity even at moderate discharge rates (over 3 or 10 k $\Omega$  load). In addition to the higher anodic capacity, it is seen that in comparison with the upper portion of the figure, the  $\text{VB}_2$  anode can sustain a higher coulombic efficiency (a higher fraction of the theoretical charge capacity) at moderate current density than the  $\text{TiB}_2$  anode. Normalized by the intrinsic capacities in accordance with Eq. 6, the  $\text{TiB}_2$  anode sustains 56% of the intrinsic capacity over the 3 k $\Omega$  discharge load and approaches 70% at a 10 k $\Omega$  discharge, whereas the  $\text{VB}_2$  sustains 91% of the intrinsic capacity at 3 k $\Omega$ , which increases to 94% of the intrinsic  $11\text{e}^-$  capacity during a 10 k $\Omega$  discharge.

Figure 3 compares the discharge of alkaline electrolyte cells containing various cathode and anode couples, including  $\text{MnO}_2/\text{Zn}$  and metal hydride cells. One societal driving force for the continued use of  $\text{MnO}_2/\text{Zn}$  chemistry is the several generations of devices which have been designed for the normal operative domain of the  $\text{MnO}_2/\text{Zn}$  battery. The conventional metal hydride and alkaline



**Figure 3.** High-capacity boride or conventional alkaline anodes. Electrolyte and cell conditions are as described in Fig. 1, discharged under the indicated constant ohmic load conditions. Comparison of  $\text{TiB}_2$  and Zn or MH alkaline anodes. Cells contain excess cathode capacity and are limited to 10 mAh anode capacity. Cells discharged include  $\text{MnO}_2\text{-Zn}$  and  $\text{NiOOH-MH}$  conventional alkaline cells, as well as the Zn or MH anodes, instead of with a Fe(VI) cathode (containing 75%  $\text{K}_2\text{FeO}_4$ , 20% graphite, and 5% KOH). Other cells contain the same cathodes but a  $\text{TiB}_2$  anode instead of Zn or MH anodes.  $\text{TiB}_2$  anode: 75%  $\text{TiB}_2$ , 20% graphite, 4.5% KOH, and 0.5% binder (T-30, 30% Teflon).

$\text{MnO}_2/\text{Zn}$  cells are both seen to generate an initial discharge voltage of 1.2–1.5 V. The metal hydride cell has an anode capacity of  $\sim 300 \text{ mAh g}^{-1}$ , while the  $\text{MnO}_2/\text{Zn}$  alkaline battery approaches  $800 \text{ mAh g}^{-1}$ . It is evident in the figure that a new, alternative  $\text{MnO}_2/\text{boride}$  cell can sustain a substantially larger anode capacity. The potential of this alkaline  $\text{MnO}_2/\text{boride}$  cell is approximately 0.25 V lower than that of the conventional  $\text{MnO}_2/\text{Zn}$  or metal hydride cells. However, the alkaline thermodynamic potential of the super-iron cathode, which undergoes a  $3\text{e}^-$  reduction  $\text{Fe(VI)} \Rightarrow \text{III}$ , can compensate for this loss, as it occurs at a value of 0.25 V higher than the  $1\text{e}^-$  reduction of  $\text{MnO}_2$  (SHE = the standard  $\text{H}_2$  electrode potential):

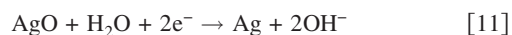


The additional potential of the Fe(VI) cathode in Eq. 9 compared to Eq. 10 is sufficient to compensate for the low voltage of the  $\text{MnO}_2/\text{boride}$  cell observed in Fig. 3. As seen, the super-iron/boride couple, respectively, with either a  $\text{TiB}_2$  (Fig. 2 top and Fig. 3) or  $\text{VB}_2$  (Fig. 2 bottom) anode, generates a discharge potential similar to the conventional alkaline  $\text{MnO}_2/\text{Zn}$  cell.

A standard oxidation potential for the  $\text{TiB}_2$  and  $\text{VB}_2$  reactions has been included in Eq. 6 and 8, which have not been previously available and which we have calculated based on literature thermodynamic values.<sup>13,14</sup> The 0.07 V differential between these values is consistent with the slightly lower potentials we measure in  $\text{VB}_2$  compared to  $\text{TiB}_2$  cells, although the respective calculated standard reduction potentials for these cells of  $-1.67$  and  $-1.74$  V vs SHE is considerably lower than the value of approximately  $-1.0$  V vs SHE that we would estimate based on our measured value of the open-circuit potential of these half reactions. This difference is equivalent to a large overpotential, and we observe that the oxidation reaction is highly irreversible. The smooth, steady discharge voltage throughout discharge of  $\text{VB}_2$  is fascinating; this may be the only example of a molecule that appears to undergo an observed, full  $11\text{e}^-$  electro-

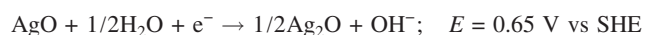
chemical oxidation at a singular potential. Further studies are needed to understand the large difference between the thermodynamic and experimental potentials, but we suggest it is related to an averaging effect of the highly multielectron character of the oxidation reaction.

A variety of alkali and alkaline earth Fe(VI) (super-iron) salts, which sustain a  $3e^-$  reduction in alkaline media at potentials consistent with Eq. 9, have been considered as alkaline cathodes.<sup>15-17</sup> Of these salts, pure  $BaFeO_4$  sustains the highest rates of cathodic reduction but is susceptible to decomposition in the solid state; furthermore, the barium salts are problematic from a toxicological perspective.<sup>17,18</sup> The potassium Fe(VI) salt,  $K_2FeO_4$ , provides several advantages. It is stable in the solid state, and its discharge product is environmentally benign. Furthermore, it has a higher cathodic capacity (406 compared to 313  $mAh\ g^{-1}$ ) than  $BaFeO_4$ , which is significantly higher than the conventional alkaline cathode  $MnO_2$  (308  $mAh\ g^{-1}$ ). Pure  $K_2FeO_4$  does not sustain the high rates of cathodic reduction observed with  $BaFeO_4$  cathodes. However,  $K_2FeO_4$  cathodes with hydroxide or manganese salts as possible additives, and in particular with silver oxide additives, can substantially enhance the rate of Fe(VI) reduction and facilitate and sustain high cathodic current densities.<sup>6,18,19</sup> An AgO additive strongly facilitates Fe(VI) cathodic charge transfer. The pure (AgO-free)  $K_2FeO_4$  cathode in Fig. 1 required 25 wt % graphite to ensure conductivity and effective cathode charge transport. The  $K_2FeO_4$  cathode with 5 wt % added KOH to facilitate charge transfer in Fig. 2 required only 20 wt % graphite to ensure effective cathode charge transport. The addition of AgO substantially facilitates Fe(VI) cathodic charge transfer and necessitates considerably less graphite in the cathode mix. With only 8.5 wt % of AgO added to the  $K_2FeO_4$  cathode, only 10 wt % graphite is required as the conductive media and still yields a greater discharge capacity (over 80% of the intrinsic cathode capacity) than a pure  $K_2FeO_4$  cathode containing 25% graphite (which yields only 70% coulombic efficiency). A pure  $K_2FeO_4$  cathode containing only 10% graphite yields only 50% coulombic efficiency under the same discharge conditions. Also, at high discharge rates, these low levels of AgO retain this higher relative fraction of the intrinsic capacity compared to AgO-free cells.<sup>18</sup> A composite cathode containing a 9:1 ratio of  $K_2FeO_4$  to AgO has an intrinsic cathodic capacity of 408  $mAh\ g^{-1}$ , as determined from  $K_2FeO_4$ 's 406  $mAh\ g^{-1}$ , and the 432  $mAh\ g^{-1}$  capacity of pure AgO, determined from its  $2e^-$  alkaline cathodic reduction of



In Fig. 4, it is seen that increasing an AgO additive in a composite  $K_2FeO_4$  cathode also substantially improves its charge transfer at high discharge rates. This is measured in cathode-limited cells through discharge at a constant load of 100  $\Omega$ , rather than at 1000 to 100,000  $\Omega$  loads as previously examined in the cells in Fig. 2. At this high rate of discharge, the composite cathode yields over four times the cathode capacity with a large fraction of added AgO as the capacity realized without the additive.

In Fig. 5 it is seen that a relatively low level of added AgO (8.5 wt %) sustains a high coulombic efficiency over a wide range of current densities. The cathode contains a fixed composition of 76.5%  $K_2FeO_4$ , 8.5% AgO, and 5% KOH. The beneficial characteristics of this cathode can be effectively coupled with the high-capacity  $TiB_2$  anode. The accessible depth of discharge of this composite cathode is over 80% and drops to 45% of the intrinsic capacity in the most rapidly discharged cell (at the 100  $\Omega$  load). The elevated voltage plateau evident in the initial <10% of the discharge, particularly at lower rates (higher discharge load conditions), occurs only in the AgO composite Fe(VI) cathodes. This plateau reflects the higher alkaline redox potential of the Ag(II) to Ag(I), compared to the Ag(I) to Ag(0) reduction



[12]

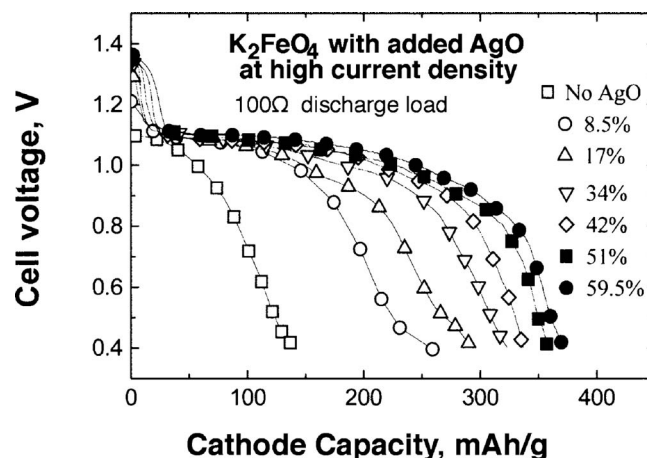


**Figure 4.** High current density discharge of composite  $K_2FeO_4$  with AgO cathode- $TiB_2$  anode cells. The cathodes are discharged under a constant 100  $\Omega$  load in 1 cm coin cells with excess intrinsic anode capacity. As indicated in the figure, the fraction of the AgO cathode additive ranges from 0 to 59.5 wt %. The cathode is prepared with a total of 29 mg of the  $K_2FeO_4$  + AgO and also contains 5% KOH and 10% graphite. Electrolyte: saturated KOH.  $TiB_2$  anode: 75%  $TiB_2$ , 20% graphite, 4.5% KOH, and 0.5% binder (T-30, 30% Teflon). The measured cathode capacity to 0.6 V discharge for the 8.5, 17, 34, 42, 51, or 59.5% AgO cells is 115, 212, 253, 298, 321, 343, or 355  $mAh/g$ .



[13]

As seen on the right sides of Fig. 6 and 7, the Fe(VI) cathode discharges to higher capacity compared to  $MnO_2$ ,  $NiOOH$ , and  $KIO_4$  alkaline cathode under equivalent cell conditions. Both figures present results utilizing the composite super-iron cathode (76.5%  $K_2FeO_4$ , 8.5% AgO, 5% KOH, and 10% g). As seen on the left side of the figures, this Fe(VI) cathode also provides a higher potential match for the boride anode than other cathodes and results in a discharge voltage domain which is similar to that of conventional alkaline and metal hydride batteries. The anodic capacity of the

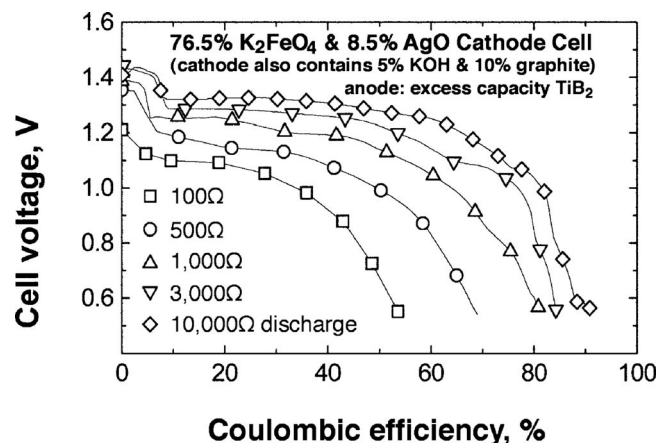


**Figure 5.** Discharge-voltage profiles, at a range of discharge loads, of fixed-composition composite  $K_2FeO_4$  (zirconia-coated)/AgO- $TiB_2$  button cells. Excess capacity  $TiB_2$  anode is prepared as 75%  $TiB_2$ , 20% graphite, 4.5% KOH, and 0.5% binder (T-30, 30% Teflon). Composite cathode is prepared with 29.5 mg 76.5%  $K_2FeO_4$ , 8.5% AgO, 5% KOH, and 10% graphite. The cells are discharged at various constant loads at 22°C. The measured coulombic efficiency to 0.6 V discharge for the cell discharge at these loads of 100, 500, 1000, 3000, or 10,000  $\Omega$  is 52, 67, 80, 83, or 87%.

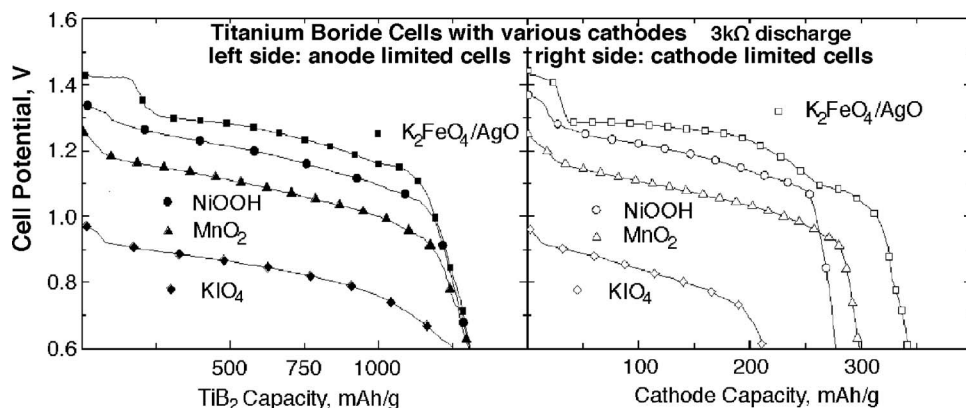
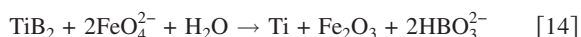
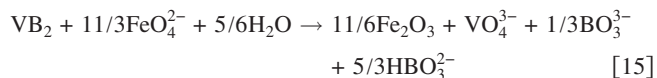


**Figure 6.** Titanium boride anodes discharged coupled with a variety of alkaline cathodes under (left) anode-limited and (right) cathode-limited conditions. Anode: 75 wt %  $\text{TiB}_2$ , 20% g, 4.5% KOH, and 0.5% binder (T-30, 30% Teflon), g = 1  $\mu\text{m}$  graphite. The cathode is either  $\text{K}_2\text{FeO}_4$ ,  $\text{MnO}_2$ ,  $\text{NiOOH}$ , or  $\text{KIO}_4$  or, more specifically, 76.5%  $\text{K}_2\text{FeO}_4$ , 8.5%  $\text{AgO}$ , 5% KOH and 10% g; 90%  $\text{MnO}_2$  and 10% g;  $\text{NiOOH}$ ; or 75%  $\text{KIO}_4$  and 25% g. Anode- and cathode-limited conditions are studied by packing each cell, respectively, with excess intrinsic cathode or anode capacity. Electrolyte and cell construction are as described in Fig. 1; cells are each discharged at a constant 3 k $\Omega$  load.

titanium boride anode in Fig. 6 is substantially higher than that of zinc. The discharge reaction for the super-iron/titanium boride full cell is derived through Eq. 6 and 9

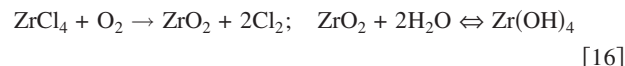


The observed  $\text{VB}_2$  anode capacity of  $\sim 4000 \text{ mAh g}^{-1}$  represents an increase even higher than that of  $\text{TiB}_2$ . The electrochemical energy storage of super-iron boride including the  $11e^-$  reduction per molecule of  $\text{VB}_2$ , is diagrammatically represented in Scheme 1. As seen on the left side of Fig. 7 for an  $\text{VB}_2$ , rather than a  $\text{TiB}_2$  anode, the Fe(VI) again provides a good potential match with conventional alkaline systems, and the anodic capacity of the vanadium boride anode is now severalfold higher than that of zinc ( $800 \text{ mA g}^{-1}$ ). The overall discharge reaction for the super-iron/vanadium boride full cell is derived from Eq. 8 and 9



Boride salts can be unstable in alkaline solution.  $\text{TiB}_2$  visibly reacts on contact with KOH electrolyte (evolving  $\text{H}_2$  gas). This is not only a chemical loss of the electrochemical capacity but is flammable. In addition, due to the evolved gas, a sealed battery swells or even cracks during storage. Unlike uncoated titanium boride, we recently demonstrated that a 1% zirconia-coated  $\text{TiB}_2$  does not evolve hydrogen.<sup>7</sup> A 1% zirconia-coated  $\text{TiB}_2$  is equivalent to a 0.1  $\mu\text{m}$   $\text{ZrO}_2$  overlayer on a 30  $\mu\text{m}$  diameter  $\text{TiB}_2$  particle. Zirconia is insoluble and extremely stable in aqueous alkaline media.<sup>20,21</sup> Based on our previous experience (Mn coating<sup>10</sup>), we recently developed a zirconia overlayer which is derived from an organic soluble zirconium salt ( $\text{ZrCl}_4$ ) via an organic medium.<sup>6</sup> In this study, high-capacity boride anodes are modified with this zirconia coating methodology.

As seen in Fig. 8, similar to the coated cathode materials,<sup>6</sup> ATR/FTIR analysis reveals the zirconia 1396 and 1548  $\text{cm}^{-1}$  peaks on a variety of coated materials. This includes the coated active anode materials  $\text{TiB}_2$  and  $\text{VB}_2$ , as well as coated cathode materials, such as  $\text{K}_2\text{FeO}_4$  and  $\text{AgO}$ . Pure  $\text{ZrO}_2$  is prepared (as a colloid) for comparison, and the two absorption peaks coincide with the absorption spectra of zirconia.<sup>6,22</sup> The conversion of  $\text{ZrCl}_4$  to zirconia forms a pure  $\text{ZrO}_2/\text{Zr}(\text{OH})_4$ , depending on the extent of hydration



The discharge of the complete super-iron titanium boride redox chemistry is investigated in Fig. 9 using cells with balanced  $\text{TiB}_2$  anode and Fe(VI) cathode capacity (based on the intrinsic capacity of the anode and cathode components). The capacity is determined from the integrated charge, normalized by the sum of the total active anode ( $\text{TiB}_2$ ) and cathode ( $\text{K}_2\text{FeO}_4$  and  $\text{AgO}$ ) components. Alkaline redox couples are prepared in an electrochemical coin cell configuration and are studied with or without a zirconia coating in this figure. The reaction products depend on the depth of discharge, pH, and the degree of dehydration of the boric and ferric products, and the cell may be generalized in the representative deep discharge reaction. As determined from Eq. 14, the theoretical capacities for the complete super-iron/ $\text{TiB}_2$  (6F per  $\text{TiB}_2 + 2\text{K}_2\text{FeO}_4$ ) cell is  $345 \text{ mAh g}^{-1}$ .

The electrochemical stability of  $\text{K}_2\text{FeO}_4$  is dramatically improved by a 1%  $\text{ZrO}_2$  coating, and an 8.5 wt %  $\text{AgO}$  additive further facilitates the cathode charge transfer. The zirconia overlayer provides an ionic-conductive, alkaline stable coating which is capable of mediating hydroxide transport from the electrolyte to the electrode, and a zirconia-modified  $\text{K}_2\text{FeO}_4/\text{AgO}$  composite cathode exhibits longevity and high charge-storage capacity.<sup>6</sup>

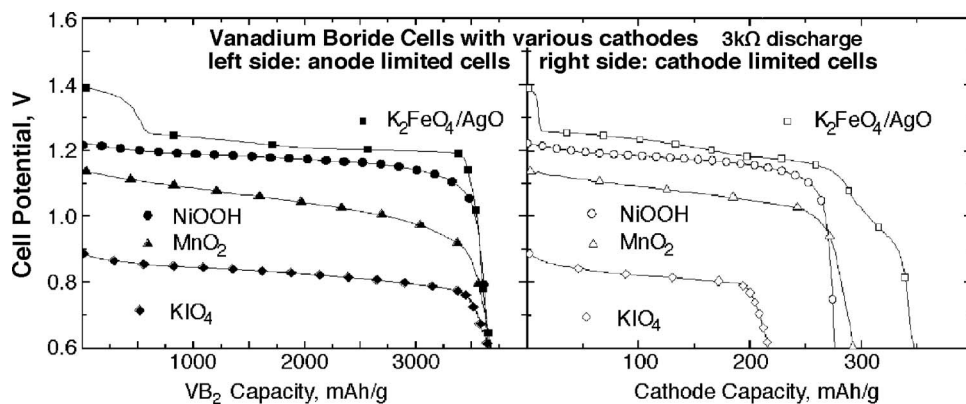
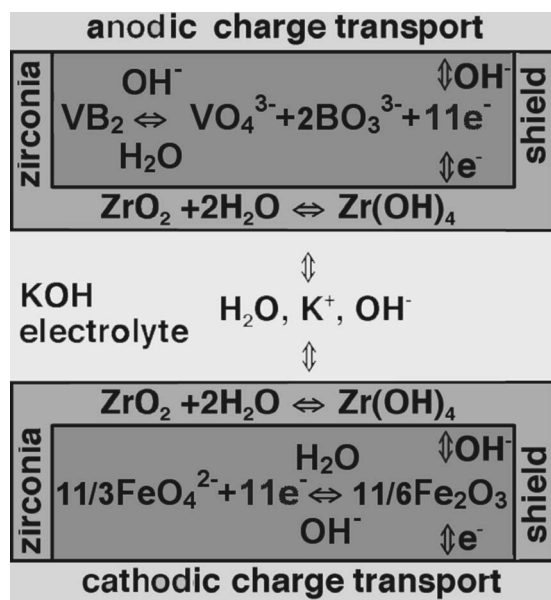


**Figure 7.** Vanadium boride anode batteries discharged with a variety of alkaline cathodes under (left) anode-limited and (right) cathode-limited conditions. Anode: 75 wt %  $\text{VB}_2$ , 20% g, 4.5% KOH, and 0.5% binder (T-30, 30% Teflon), g = 1  $\mu\text{m}$  graphite. The cathode is either  $\text{K}_2\text{FeO}_4$ ,  $\text{MnO}_2$ ,  $\text{NiOOH}$ , or  $\text{KIO}_4$ . Cathode details and cell construction conditions are described in Fig. 5; cells are each discharged at a 3 k $\Omega$  load.



**Scheme 1.** An  $11\text{e}^-$  anodic alkaline redox storage chemistry is explored based on an environmentally benign zirconia-stabilized  $\text{Fe}^{6+}/\text{B}^{2-}$  chemistry, which sustains an electrochemical potential matched to the pervasive, conventional  $\text{MnO}_2$ -Zn battery chemistry, however with a higher electrochemical capacity.

As recently demonstrated for the cathode,<sup>6</sup> this zirconia overlayer also substantially stabilizes the alkaline anode, such as the  $\text{TiB}_2$  anode.<sup>7</sup> As seen in Fig. 9, after storage, the uncoated super-iron titanium boride cell generates only 10–15% of the  $3\text{ k}\Omega$  discharge capacity of the fresh cell. In marked contrast to this, the full charge capacity is retained when zirconia-coated super-iron and zirconia-coated boride are utilized. Instead of the uncoated electrodes, if either anode or cathode (but not both) is coated, then a fraction, but not all, of the charge capacity is lost. Also evident in the figure, the zirconia coated super-iron vanadium boride cell retains its substantial charge capacity after storage. The fundamental chemistry of conventional alkaline primary<sup>4</sup> and metal hydride rechargeable<sup>2</sup> batteries are understood and continue to be of widespread interest. The charge retention for the super-iron boride cells is already comparable to that observed in early alkaline primary cells and is better

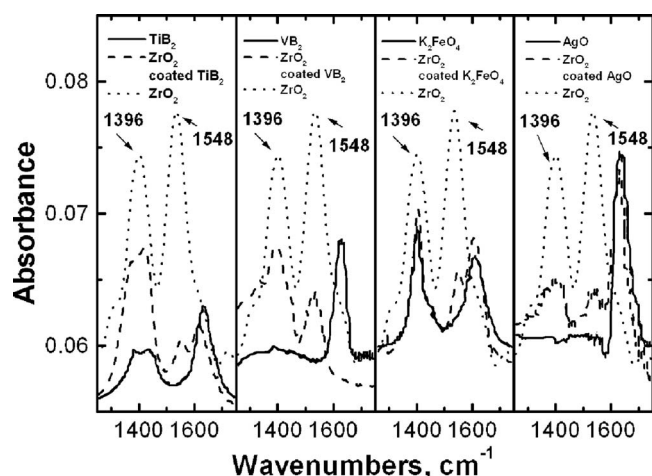


**Figure 8.** ATR/FTIR spectra of zirconia-coated and uncoated  $\text{TiB}_2$ ,  $\text{VB}_2$ ,  $\text{K}_2\text{FeO}_4$ , and  $\text{AgO}$  compared with the pure  $\text{ZrO}_2$  spectra. Spectra of 5% coated salts are included for emphasis; a 1% zirconia coating exhibits evident but proportionally smaller  $1396$  and  $1548\text{ cm}^{-1}$  peaks.

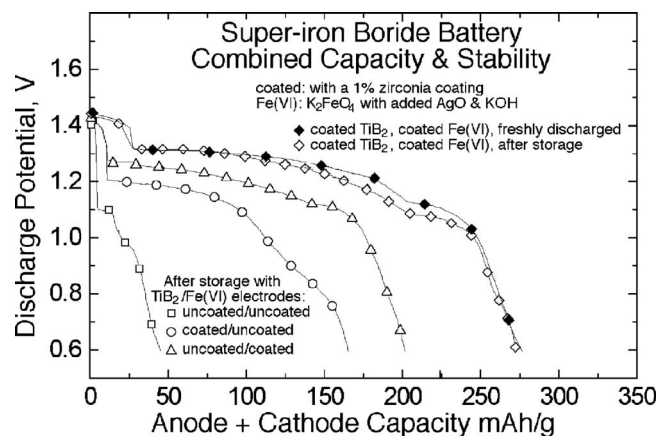


**Figure 9.** Capacity (anode + cathode) of the super-iron  $\text{TiB}_2$  boride alkaline battery compared to that of the conventional (manganese dioxide/zinc) alkaline battery. The super-iron boride cell is prepared with a 76.5%  $\text{K}_2\text{FeO}_4$ , 8.5%  $\text{AgO}$ , 5%  $\text{KOH}$ , and 10%  $1\text{ }\mu\text{m}$  graphite cathode and a  $\text{TiB}_2$  anode, as indicated in the figure. The cells are discharged at a constant load of  $3\text{ k}\Omega$  at  $22^\circ\text{C}$ . Charge retentions (stability) of the cells are compared when freshly discharged and after 1 week of storage at  $22^\circ\text{C}$ , with or without a 1% zirconia coating applied to the  $\text{Fe(VI)}$  or boride salts.

than that of contemporary alkaline rechargeable cells. In addition to the stability of the super-iron  $\text{VB}_2$  cell presented in Fig. 10 at room temperature, we observe that the vanadium boride anode exhibits higher stability than the titanium boride anode. Accelerated long-term stability is measured at higher temperatures. Without the zirconia overlayer, after 1 week of storage the vanadium boride anode retains 90% of the original charge capacity at  $45^\circ\text{C}$  (100% after 1 week with the zirconia coating) and 65% of the charge capacity at  $70^\circ\text{C}$  (85% with zirconia). We have previously demonstrated the extended long-term solid-state stability of several alkali super-iron salts at these temperatures<sup>16</sup> and have recently studied the variation of the coating level and particle size and demonstrated longer-term  $\text{Fe(VI)}$  cathode stability conditions.<sup>23</sup>

The capacity range of the conventional alkaline Zn– $\text{MnO}_2$  cell is included as dashed vertical lines in Fig. 10, which show the range from a maximum experimental ( $<160\text{ mA/g}$ ) to a theoretical ( $2\text{F per Zn} + 2\text{MnO}_2 = 222\text{ mAh g}^{-1}$ ) charge storage capacity. The super-iron boride chemistry exhibits significantly higher charge stor-

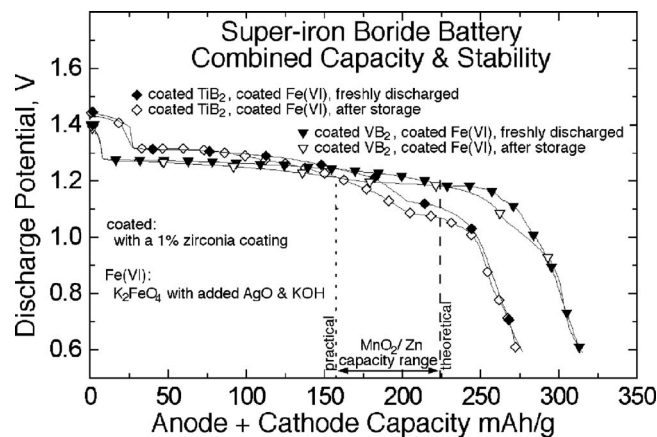


**Figure 10.** Capacity (anode + cathode) of the super-iron  $\text{TiB}_2$  and a  $\text{VB}_2$  boride alkaline battery. The super-iron boride cell is prepared with a 76.5%  $\text{K}_2\text{FeO}_4$ , 8.5%  $\text{AgO}$ , 5%  $\text{KOH}$ , and 10%  $1\text{ }\mu\text{m}$  graphite cathode and either a  $\text{TiB}_2$  or a  $\text{VB}_2$  anode, as indicated in the figure. Charge retentions (stability) of the cells are compared when freshly discharged and after 1 week of storage, with a 1% zirconia coating applied to the  $\text{Fe(VI)}$  and boride salts.

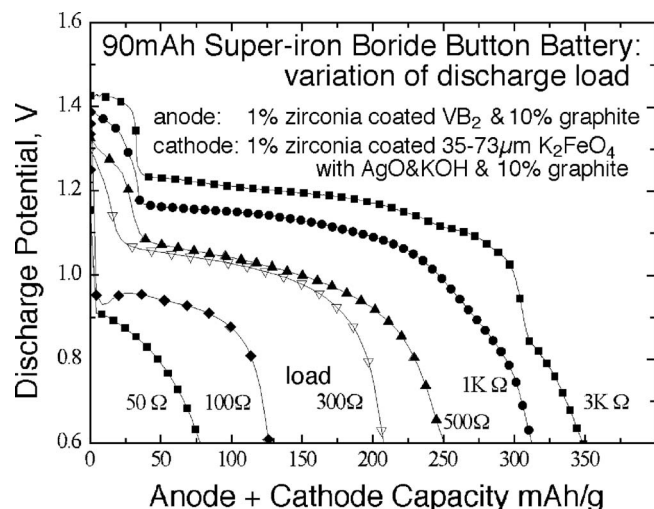


**Figure 11.** Discharge of the 90 mAh vanadium boride super-iron battery at various discharge loads. Anode (90 mAh):  $\text{VB}_2$  (1% Zr coated; 90 wt %) + graphite (1  $\mu\text{m}$ , 10 wt %); cathode (100 mAh):  $\text{K}_2\text{FeO}_4$  (1% Zr-coated; 35–73  $\mu\text{m}$ ; 76.5 wt %) + AgO (8.5 wt %) + KOH (5.0 wt %) + graphite (1  $\mu\text{m}$ , 10 wt %); electrolyte: saturated KOH solution.

age than conventional alkaline primary storage chemistry. As determined from Eq. 15, the theoretical capacity for the complete super-iron/ $\text{VB}_2$  (11F per  $\text{VB}_2$  + 11/3 $\text{K}_2\text{FeO}_4$ ) cell is 369 mAh  $\text{g}^{-1}$ . As seen in the figure, the super-iron titanium boride cell combined anode and cathode capacity is experimentally in excess of 250 mAh  $\text{g}^{-1}$ , and that of the super-iron  $\text{VB}_2$  cell is over 310 mAh  $\text{g}^{-1}$ , which is two-fold higher than that of the conventional alkaline battery chemistry ( $\text{MnO}_2/\text{Zn}$ ).

Figure 11 explores the super-iron boride ( $\text{VB}_2$ ) battery as prepared with a higher, more functional storage capacity. The anode and cathode active components of the 1 cm button (coin) cell configuration are increased by an order of magnitude to 90 and 100 mAh of the respective intrinsic capacities of the anode and cathode capacities. The higher capacity (100 mAh) of the super-iron cathode is in line with the marginally lower coulombic efficiency (in excess of 80% of the intrinsic capacity, compared to in excess of 90% for the anode) observed at the 3 k $\Omega$  discharge. The anode is composed of 90 wt %  $\text{VB}_2$  and 10% 1  $\mu\text{m}$  graphite. The cathode is composed of 76.5 wt %  $2\text{K}_2\text{FeO}_4$ , 8.5% AgO, 5% KOH, and 10% graphite. As seen in the figure, the capacity of the cell exceeds 320 mA  $\text{g}^{-1}$  at the 3 k $\Omega$  discharge, based on these active materials. Further enhancement, particularly in terms of optimization of the particle size within the anode and cathode, and also the electrolyte composition, is expected to further improve the capacity and sustainable current density, while a determination of capacity inclusive of nonactive components (graphite and zirconia mass, case, etc.) will decrease the practical capacity.

### Conclusion

Whereas a conventional alkaline battery pairs the  $2e^-$  zinc anode and  $1e^-$   $\text{MnO}_2$  cathode, the alkaline super-iron/boride cell pairs up to an  $11e^-$  boride anode, such as  $\text{VB}_2$ , and a  $3e^-$  hexavalent iron cathode. The super-iron boride chemistry exhibits significantly

higher charge storage than conventional alkaline primary storage chemistry while sustaining an electrochemical potential (under both open-circuit and discharge conditions) matched to this pervasive, conventional  $\text{MnO}_2$ -Zn battery chemistry. The  $\text{VB}_2$  anode capacity (4060 mAh  $\text{g}^{-1}$ ) and  $\text{K}_2\text{FeO}_4$  cathode capacity (408 mAh  $\text{g}^{-1}$ ) are considerably higher than that of Zn and  $\text{MnO}_2$ , or NiOOH, in conventional alkaline batteries. Based on  $\text{VB}_2$  (72.6 g  $\text{mol}^{-1}$ ) and the Fe(VI) salt  $\text{K}_2\text{FeO}_4$  (198.0 g  $\text{mol}^{-1}$ ), the complete super-iron boride cell has an 11 Faraday theoretical capacity of 369 mAh  $\text{g}^{-1}$  (or 371 mAh  $\text{g}^{-1}$  when a cathode also contains 1 part AgO to 9 parts  $\text{K}_2\text{FeO}_4$ ; the added AgO mediates and facilitates the  $3e^-$   $\text{K}_2\text{FeO}_4$  charge transfer). We demonstrate that this intrinsic capacity is approached experimentally and is substantially higher than the conventional Zn/ $\text{MnO}_2$  alkaline battery with a theoretical capacity of 224 mAh  $\text{g}^{-1}$  and an experimental capacity (to 0.8 V) of 160 mAh  $\text{g}^{-1}$ .

A further optimization of both the boride and super-iron salt particle size, coupled with study and variation of the zirconia coating, may further enhance cell performance. Alternate metal borides, as well as alternate super-irons, also affect characteristics of the super-iron boride cell capacity, and ongoing studies of the charge transfer of these unusual cathode and anode salts will impact, and may be expected to lead to, further enhancements of charge transfer, retention, and capacity of the super-iron boride chemistry.

### Acknowledgment

This program is supported in part by the U.S. Department of Energy and the University of Massachusetts through the CVIP Technology Development Fund.

### References

- S. Licht, B. Wang, and S. Ghosh, *Science*, **285**, 1039 (1999).
- S. R. Ovshinsky, M. Fetchenko, and J. Ross, *Science*, **260**, 176 (1993).
- J. R. Dahn, T. Zheng, Y. Liu, and J. S. Xue, *Science*, **270**, 590 (1995).
- Z.-R. Tian, W. Tong, J.-Y. Wang, N.-G. Duan, V. Krishnan, and S. L. Suib, *Science*, **276**, 926 (1997).
- S. Licht and R. Tel-Vered, *Chem. Commun. (Cambridge)*, **2004**, 628.
- S. Licht, X. Yu, and D. Zheng, *Chem. Commun. (Cambridge)*, **2006**, 4341.
- S. Licht, X. Yu, and Y. Wang, *Chem. Commun. (Cambridge)*, **2007**, 2753.
- H. X. Yang, Y. D. Wang, X. P. Ai, and C. S. Cha, *Electrochem. Solid-State Lett.*, **7**, A212 (2004).
- Y. D. Wang, X. P. Ai, Y. L. Cao, and H. X. Yang, *Electrochem. Commun.*, **6**, 780 (2004).
- S. Licht, V. Naschitz, B. Liu, S. Ghosh, N. Halperin, L. Halperin, and D. Rozen, *J. Power Sources*, **99**, 7 (2001).
- S. Licht, V. S. Licht, V. Naschitz, L. Halperin, N. Halperin, L. Lin, J. Chen, S. Ghosh, and B. Liu, *J. Power Sources*, **101**, 167 (2001).
- S. Licht, L. Yang, and B. Wang, *Electrochem. Commun.*, **7**, 931 (2005).
- A. J. Bard, R. Parsons, and J. Jordan, *Standard Potentials in Aqueous Solutions*, Marcel Dekker, New York (1985).
- Property and Thermochemistry Database, [http://mole.ipe.ac.cn/all\\_thermochemistry/](http://mole.ipe.ac.cn/all_thermochemistry/) (last accessed Feb. 6, 2008).
- S. Licht, V. Naschitz, D. Rozen, and N. Halperin, *Electrochem. Commun.*, **3**, 350 (2001).
- S. Licht, V. Naschitz, D. Rozen, and N. Halperin, *J. Electrochem. Soc.*, **151**, A1147 (2004).
- S. Licht, D. Rozen, R. Tel-Vered, and L. Halperin, *J. Electrochem. Soc.*, **151**, A31 (2004).
- S. Licht, S. Ghosh, V. Naschitz, L. Halperin, and N. Halperin, *J. Phys. Chem. B*, **106**, 5947 (2002).
- S. Licht, S. Ghosh, V. Naschitz, L. Halperin, and N. Halperin, *J. Phys. Chem. B*, **105**, 11933 (2001).
- W. F. Linke, *Solubilities of Inorganic and Metal-Organic Compounds*, 4th ed., Van Nostrand, Princeton, NJ (1958).
- S. Hettiarachchi, P. Kedzierzawski, and D. D. Macdonald, *J. Electrochem. Soc.*, **132**, 1866 (1985).
- X. Fang, C. Yang, and J. Chen, *J. Chin. Ceram. Soc.*, **6**, 732 (1996).
- S. Licht, X. Yu, and Y. Wang, *J. Electrochem. Soc.*, **155**, A1 (2008).